Biophysical Journal Volume 71 November 1996 2774–2785

Mechanical Characterization of Skeletal Muscle Myofibrils

Alexander L. Friedman* and Yale E. Goldman#
Departments of *Bioengineering and #Physiology and the Pennsylvania Muscle Institute, University of Pennsylvania, Philadelphia, Pennsylvania 19104 USA

ABSTRACT A new instrument, based on a technique described previously, is presented for studying mechanics of micron-scale preparations of two to three myofibrils or single myofibrils from muscle. Forces in the nanonewton to micronewton range are measurable with 0.5-ms time resolution. Programmed quick (200-μs) steps or ramp length changes are applied to contracting myofibrils to test their mechanical properties. Individual striations can be monitored during force production and shortening. The active isometric force, force-velocity relationship, and force transients after rapid length steps were obtained from bundles of two to three myofibrils from rabbit psoas muscle. Contrary to some earlier reports on myofibrillar mechanics, these properties are generally similar to expectations from studies on intact and skinned muscle fibers. Our experiments provide strong evidence that the mechanical properties of a fiber result from a simple summation of the myofibrillar force and shortening of independently contracting sarcomeres.

INTRODUCTION

A molecular understanding of muscle contraction will require detailed correlation of the mechanical events in the contractile apparatus with the biochemistry and structural biology of actomyosin. The conventional hypothesis for energy transduction is that an internal motion, such as tilting of the myosin head while attached to actin, slides the myofilaments by 5–10 nm (Reedy et al., 1965; Huxley, 1969; Huxley and Simmons, 1971). This tilt is generally thought to be coupled to release of products (P_i and/or ADP) of ATP hydrolysis from the actomyosin complex during each enzymatic turnover (Cooke, 1986; Goldman, 1987).

Studies on the isolated proteins (Lymn and Taylor, 1971, Stein et al., 1979; Uyeda et al., 1990; Finer et al., 1994; Ishijima et al., 1994) and on single muscle fibers, particularly intact fibers of frog muscle (Huxley, 1974), permeabilized insect flight muscle (Reedy et al., 1965; 1988), and rabbit psoas muscle (Cooke et al., 1982; Ferenczi et al., 1984; Goldman et al., 1984a,b; Hibberd et al., 1985; Irving et al., 1995) have generally supported the conventional cross-bridge model, including scaling of the force and sliding distance, measured at the molecular level, up to the mechanics of the intact fiber. Some important challenges, however, have not been resolved (Harada et al., 1990; Lombardi et al., 1992).

The contractile machinery in a muscle fiber contains several thousand myofibrils arranged in parallel. Myofibrils are the smallest subdivision of the contractile apparatus retaining the normal hexagonal filament lattice, but comparatively little information is available on the detailed mechanics and biochemistry at this intermediate level. Their small size confers some experimental advantages over fibers, such as short diffusion distance, but they are harder to manipulate. Barman, Travers, and colleagues (Houadjeto et al., 1991; Herrmann et al., 1994) have shown that myofibrils are good models of fibers with respect to enzymatic activity, and they are amenable to detailed biochemical investigation.

Do the mechanical properties of the myofibrils sum in a straightforward manner to make up the behavior of the fiber? Do myofibrils normally contract independently or is there cooperation or communication between adjacent myofibrils in a fiber? Some reports in the literature suggest that myofibril activation is highly nonuniform (Bartoo et al., 1993) or that the dynamic response at test frequencies above 50 Hz is similar to a pure elasticity (Iwazumi, 1989), whereas fibers show complex viscoelasticity, related to active energy transduction, over a wide frequency spectrum (Huxley, 1974; Kawai and Brandt, 1980).

Based on a technique described by Iwazumi (1987), we built an instrument that allowed us to manipulate single myofibrils or bundles of several myofibrils and to perform detailed mechanical studies. Our instrument is less sensitive than Iwazumi's version but is less complex and enables imaging of the individual sarcomeres during contraction while simultaneously recording the mechanical response. The isometric force, relationship between force and velocity, and response to quick step changes in length were investigated in myofibrils from rabbit psoas muscle. We found that these properties generally support the hypothesis that fiber mechanics are the straightforward sum of the myofibrillar force and shortening, although we noted some discrepancies. Part of the work has been presented in preliminary form (Friedman and Goldman, 1993, 1994, 1995).

Received for publication 3 June 1996 and in final form 27 August 1996.

Address reprint requests to Dr. Yale E. Goldman, Department of Physiology, University of Pennsylvania School of Medicine, D700 Richards Bldg., 3700 Hamilton Walk, Philadelphia, PA 19104-6083. Tel.: 215-898-4017; Fax: 215-898-2653; E-mail: goldmany@mail.med.upenn.edu.

Dr. Friedman's present address: Department of Biochemistry, Stanford University, Palo Alto, CA 94305-5307.

0006-3495/96/11/2774/12 $2.00

MATERIALS AND METHODS

Principle of operation

Bundles of two or three myofibrils were glued to the bottoms of two U-shaped wire loops (Fig. 1 *A*) that were suspended in a fixed magnetic field. The positions of the bottoms of the loops were detected by photodiodes and the signals fed back through amplifiers that drove electrical current through the wire loops to clamp the positions constant or to impose programmed position steps or ramps. Each of the two wires had an independent feedback loop. When myofibrils pulled on the wire, the electrical current generated an equal and opposing force to clamp the position. The current through the wire could thus be used to measure the myofibrillar force. The relationship between force and current was given by $\mathbf{F} = I\int(\mathbf{B} \times d\mathbf{s})$, where $\mathbf{F}$ is the force vector, I is the current, $\mathbf{B}$ is the magnetic field vector, $\times$ indicates cross-product and $d\mathbf{s}$ is an infinitesimal vector defined by the path of the wire. For the present case this equation simplifies to $F = IBw$, where F, I, and B are the scalar values of force, current, and magnetic field, respectively, and w is the width (Fig. 1 *A*) of the loop.

Preparation of myofibril bundles and solutions

Myofibrils were obtained from psoas muscle of 3- to 4-kg New Zealand White rabbits. Bundles of psoas muscle fibers were dissected and then extracted in glycerol to remove membranes as described previously (Goldman et al., 1984a). After 4–11 days of storage at −22°C in 2.5 mM ATP solution (Goldman et al., 1984a), the bundles were placed in an ATP-free storage solution that contained 2.5 mM $MgCl_2$, 5 mM EGTA, 10 mM imidazole, 170 mM potassium proprionate, pH 7.0, at 0°C and glycerol, 50% v/v. The bundles were stored at −22°C for 1–11 weeks. Myofibrils or myofibrillar bundles were obtained on each day of experimentation by homogenizing (model SDT-1810 homogenizer, SDT-080E microshaft, Tekmar, Cincinnati, OH; speed 60 for 10 s) a 1 cm × 1 mm^2 segment in 1.7 ml of rigor solution. The results of homogenization were variable but typically yielded ~20 bundles of two or three myofibrils per 20 μl of suspension. Larger bundles, clumps of myofibrils and nuclei were also present. Clumps were removed by filtering through a polypropylene mesh that contained 100-μm pores (Small Parts, Miami Lakes, FL). The suspension usually yielded 50–300 μm long, fairly straight, myofibril bundles with A bands and Z lines that were clear under phase contrast microscopy (×400).

The solutions for the experiments all contained 100 mM *N*-Tris(hydroxymethyl)methyl-2-aminoethanesulfonic (TES) buffer, 10 mM reduced glutathione, 1 mM free Mg^{2+}, 200 mM total ionic strength and pH 7.1 at 20°C. Rigor solution contained additionally 3.2 mM $MgCl_2$ and 52.7 mM EGTA. Relaxing solution contained 15 mM Na_2ATP, 15.3 mM $MgCl_2$, 10 mM EGTA, and 18.2 mM 1,6-diamino-hexane-*N,N,N',N'*-tetraacetic acid (HDTA). Activating solution contained 15 mM Na_2ATP, 14.8 mM $MgCl_2$, 10 mM Ca-EGTA, ~30 μM free Ca^{2+}, and 18.5 mM HDTA. All constituents were analytical grade. Myofibril solutions were made at room temperature (20–24°C), filtered through a 0.45-μm hydrophobic nylon membrane (Lida Manufacturing Corp., Kenosha, WI), and stored at −22°C.

Instrumentation

Chamber and solution exchange

The experimental chamber was a tunnel made from two Teflon blocks attached to a glass microscope slide (Fig. 1 *B*). This assembly was lowered onto a silanized (Prosil-28; PCR Inc., Gainesville, FL) coverslip to obtain a 64-μl volume of solution contained by surface tension but with open sides that provided access for the wire loop supports and perfusion cannulas. Activating and relaxation solutions were perfused by gravity at 13–16 μl/s through parallel 0.8-mm inlet tubes and removed by gentle suction through a gold electron microscopy grid (G1000HSG; Ted Pella, Redding, CA; 20-μm holes and 5-μm bars) fixed to the end of a fluid-filled outlet tube. The chamber volume was regulated automatically by the outflow as described by Ruppersberg and Rüdel (1983). The grid was tilted ~45° relative to the solution meniscus so that increased volume in the trough wetted more grid holes, thereby increasing the outflow. More holes were active at higher flow rates. The open ports and lack of a tight seal between the chamber and the coverslip caused relatively slow (~1-10 s) exchange of solution. Hence the response of the myofibrils was limited by this mixing time within the chamber (see Fig. 3).

Optics and optoelectronics

The set-up was constructed on an inverted microscope (Fig. 1 *C*; Diaphot-TMD, Nikon, Tokyo, Japan) placed on a vibration isolation table. The

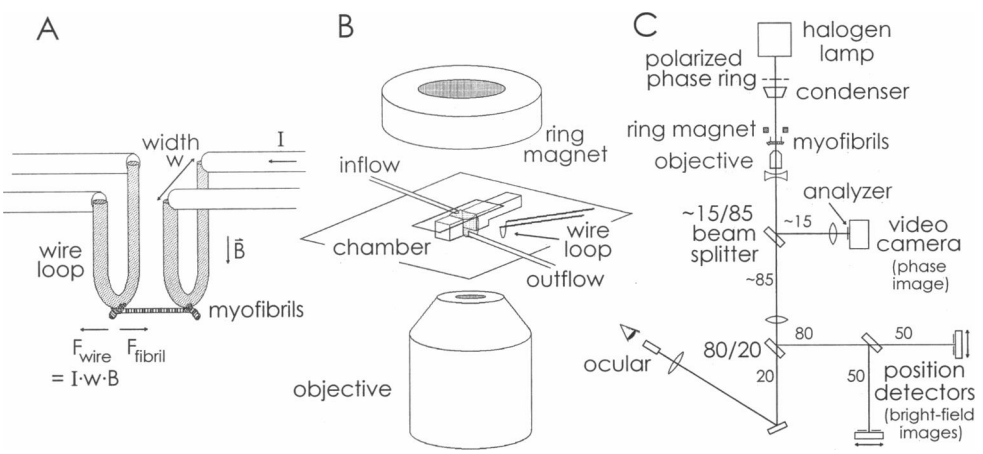

FIGURE 1 Instrumentation for mechanics measurements on myofibrils. (*A*) Principle of the method. When the myofibrils exert forces (F_{fibril}) on the wire loops, the feedback systems pass currents (I) through the loops and clamp the length constant. The electronic force (F_{wire}) is the product of I, w (width of the loops), and B (magnitude of the magnetic field vector). (*B*) Mechanical arrangement of the experimental chamber and associated components. The chamber is placed on a coverslip on the stage of an inverted microscope. The myofibrils are accessed from side openings that receive flow cannulas and wire loops. (*C*) Schematic diagram of the microscope. Four images are created by three beam-splitting prisms. A 50/50 beam splitter projects bright-field images of the wire loops onto the position detectors. The reflection and transmission ratios of the other two beam splitters are indicated in the diagram. The polarized phase ring and analyzer produce a phase image at the video camera as explained in the text.

objective (CF Achromat LWD DL 40X F, 0.55 N.A., with spherical aberration correction ring; Nikon) created images of the bottoms of the wire loops and the myofibril bundle at four separate image planes. An image of the preparation could be observed directly through the oculars. A phase image of the myofibril bundle was projected onto a CCD video camera (model VE CCD; Dage MTI, Michigan City, IN) by a relay lens that allowed independent focusing of the myofibril image at the CCD camera. A nonpolarizing 50/50 beam splitter was used to generate two bright-field images that were projected onto photodiode pairs (model PIN-Spot/2D, United Detector Technologies, Hawthorne, CA) that detected the wire loop positions.

A novel method was used to simultaneously generate the phase and bright-field images. The opaque center of the standard phase annulus in the microscope condenser was replaced with a linear polarizing disc (polarized phase ring in Fig. 1 *C*). This disc was aligned with the phase ring of the objective by viewing the back focal plane. A crossed polarizer (analyzer) was placed in front of the video camera to generate a high contrast phase image. The photodiode pairs did not have this analyzer and therefore received bright-field images of the wires.

The position signals were the difference photocurrents generated by each photodiode pair. An error signal, generated by subtracting a command voltage from the position signal, was fed to power amplifiers that drove current through the wires to clamp positions. The dynamic response of each servo loop was adjusted using integral, proportional, velocity, and acceleration feedback. One wire was used primarily for force detection and the other for imposing length changes. The optimal settings of the dynamic response were altered for these two tasks.

The loops were formed from 12-μm-diameter pure platinum wire (<0.001% impurities; California Fine Wire Co., Grover City, CA). A device was built to conveniently form the loops around a 2-mm polished cylinder and to weld them onto 440-μm-diameter platinum support rods. A 2-mm-long by 2-mm-wide loop of platinum wire had a natural resonant frequency of ~600 Hz. The feedback electronically increased the resonant frequency to 1–2.5 kHz, leading to step responses (5–95%) of 200–500 μs. The rms noise of the force transducer was 10 nN, DC to 1.4 kHz. A small degree of optical and electrical cross-talk between the servo systems was corrected by subtracting force recordings during relaxation from those during activation.

The magnetic field was provided by a cobalt ring magnet (Edmund Scientific, Barrington, NJ). The maximal field strength was measured to be 240 Gauss by applying current through a wire loop with known mechanical compliance and recording the deflection. The myofibrils were placed in the position of maximal field strength. The field was uniform to within 1% in the volume occupied by the myofibrils. To calibrate the force transducer, a cantilever wire of known compliance was pressed against the wire loop to apply a known force, and the current that returned the loop to its null position was measured. The response was linear up to at least 4.8 μN.

The chamber, magnet, flow cannulas, and wire loops were mounted on manipulators that attached to a circular track attached to the microscope stage (Orbital Stage System, Meridian Manufacturing, Kent, WA). Hydraulic manipulators (model NO-188, Narishige Co., Tokyo, Japan) positioned the wire loops during the mounting of a myofibril.

Experimental protocol

Attachment of a selected myofibril bundle to the wire loops

A 20-μl drop of the filtered suspension of rigor myofibrils was transferred to the microscope stage for selection of the myofibrillar bundle. Clumps of myofibrils or larger pieces of tissue in the suspension were removed if necessary with fine tungsten needles (model PTT-06, Alessi, Irvine, CA). A myofibril bundle was chosen that was segregated from other objects and had clear, transverse striations. Bundles used were 90–200 μm long, and appeared to contain three or fewer myofibrils. It was important that a bundle was free from the coverslip over most of its length so that it could detach from the coverslip without being damaged by adhesion. The end of a loop was coated with glue (3145 RTV, Dow Corning, Midland, MI), quickly inserted into the solution chamber, manipulated down to press the glue onto the bundle, and left in that position for 60 s while the glue set. The loop with attached myofibril was slowly raised off of the coverslip and the myofibril was pulled free of the glass surface. The attached end of the bundle was re-lowered near to the surface and the gluing procedure was repeated for the other end. Both loops were then raised 250 μm above the coverslip to facilitate solution exchange and to minimize contamination from surface debris. The loops were translated to center the bundle on the optic axis. The bundle, mounted in the rigor state, was then relaxed by flowing 15 mM Mg-ATP solution through the chamber. Unless otherwise stated, the sarcomere length of the bundle obtained after relaxation (typically 2.2–2.6 μm) was used for the remainder of the experiment. Bundles longer than 80 μm before mounting were required for independent detection of the wire positions. In the experiments reported, 20–42 sarcomeres were suspended between the wires.

Mechanical measurements

Experiments were performed at room temperature (18–24°C). To initiate contraction, the inflow was switched from relaxing solution (10 mM EGTA) to activating solution (~30 μM free calcium). After a short period of solution mixing, tension developed and achieved a steady value (Fig. 3). A mechanical perturbation, such as a length step or ramp, was applied during steady contraction and, approximately 2 s later, the flow was switched back to relaxing solution. The bundle was returned to its original length after relaxation was complete. Various length steps or ramp speeds were applied in successive activations; the order of the ramp speeds or of the length-step amplitudes was randomized to compensate for altered performance in successive contractions.

Data collection and analysis

The video signal from the CCD camera was recorded and stored in S-VHS format (model SLV-R5UC VCR, Sony, Park Ridge, NJ). The sarcomere length was measured from the video signal played back on the VCR. An individual video line representing the myofibrillar sarcomeres (Fig. 2, *A* and *B*) was isolated from the raster using either a video synch separator (LM1881N, National Semiconductor Corp., Santa Clara, CA) and timing chip, or the event-counting trigger mode of a digital storage oscilloscope (model Pro 40, Nicolet, Madison, WI). The length of an individual sarcomere, or the average length of several sarcomeres, was measured from the distance between intensity peaks representing I bands. This method provided a short time aperture for measuring sarcomere length (a horizontal sweep occupies 63.5 μs), but successive measurements were limited to the 17- or 33-ms field or frame rates of the NTSC video standard.

The tissue-glue interface was assumed to be midway between the center of the wire and the surface of the glue closest to the optic axis (Fig. 2). Muscle length was defined as the distance between the two tissue-glue interfaces. The cross-sectional area of each preparation was obtained from the width of the myofibril bundle in the video image assuming that the bundle approximates a pair or triplet of parallel right cylinders. The cross-sectional area of a typical bundle was 6.0 μm^2.

Timing pulses that initiated the mechanical perturbation and triggered the data acquisition were supplied by a Z8 microprocessor-based, digital pulse generator developed in-house. The current (proportional to force) and position signals of the two wire servos were recorded at a slow time base on a four-channel chart recorder. The four signals, plus the command signal, were also amplified, digitized at 12-bit, 50- or 250-μs resolution, and stored on diskettes using an 80386-based microcomputer. For the length-step experiments a digital oscilloscope (model 3091, Nicolet) recorded the current through the force transducer wire and its position at 10-μs time resolution. These data were stored on diskettes using an 80286-based microcomputer. The ratio of sampling rates for the two digitizers was carefully checked. For display and analysis, the force signals were filtered once or twice through a 21-point Savitszky-Golay (1964)

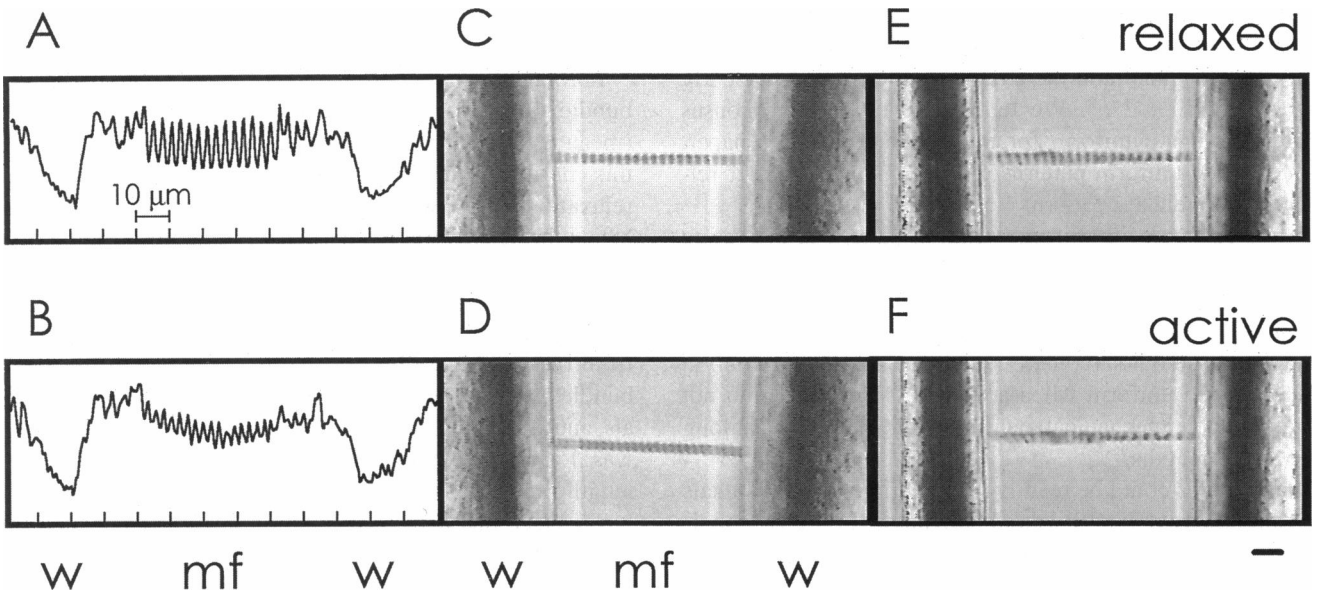

FIGURE 2 Video signal intensity and video images of mounted myofibrils. The left panels show video intensity from a video line containing the myofibril image of a relaxed (*A*) and active (*B*) bundle of three rabbit psoas myofibrils. Higher intensity is plotted upward. The wires (w) produce deep troughs and the myofibril striations (mf) produce an oscillating signal. Sarcomere length was measured from these types of signals from the distance between peaks, representing I bands; typically, the average spacing was measured from the total length occupied by 10 I bands in relaxed bundles and 5–10 I bands in active bundles. The video image that generated the signal in *A* is shown in *C*; the image that generated *B* is shown in *D*. (*E* and *F*) A different myofibrillar bundle in relaxation and contraction. Relaxed bundles (*C* and *E*) have a fairly uniform distribution of sarcomere lengths. Activated bundles (~30 μM free [Ca^{2+}]) either maintain uniformity (*D*) or become disordered (*F*). Scale bar (lower right), 10 μm.

digital low-pass filter. This filter reduced noise but did not appreciably alter the observed rate processes.

For each experimental trial, the isometric force was measured immediately before the mechanical perturbation. To correct for drift in the force signal, the baseline was taken as the average force in relaxing solution before and after the activation.

Using the Levenberg-Marquardt method (Press et al., 1992) incorporated into a program written in-house, a sum of exponential functions was fit to the dual time-base recording from each of the force transients after length steps in activating solution. The 50- or 250-μs time resolution data were characterized by a sum of two exponential functions. The data collected at 10-μs time resolution was fit by the exponential function defined by the slower data plus one faster exponential component. The stiffness of the preparation was given by dividing the change in force by the imposed step change in myofibril length. The force change was taken as the isometric force minus the value of the fitted exponential curve at the instant when the imposed step was 95% complete.

In experiments with imposed length ramps, the force varied during the ramp as described later (see Fig. 5). To determine the force-velocity curve, the force recording was extrapolated back to the beginning of the ramp. Hill's (1938) hyperbolic relation, $(P + a) \times (V + b) = (1 + a)b$, where P is the back-extrapolated force relative to isometric force, V is the imposed velocity of shortening, and a and b are constants, was fit to the data using the Levenberg-Marquardt algorithm to minimize the sum of squared velocity residuals. The maximal velocity of shortening (V_{max}) is given by b/a.

RESULTS

Sarcomere length uniformity and shortening during force development

Rigor and relaxed states

Myofibrils, prepared by homogenizing bundles of fibers in rigor, were attached to wire loops as described in Materials and Methods. The striations were very clear and uniform in rigor with sharp transitions between the A bands and I bands. If the wires were moved together, the striations did not shorten, but instead, the rigor bundles buckled. Z lines were apparent in the phase image observed through the oculars but were not preserved by the video imaging system.

When the 15 mM Mg-ATP relaxing solution was perfused through the chamber, the myofibrils relaxed smoothly with little axial motion or local stretching of sarcomeres. The striations remained uniform (Fig. 2 *C*). Relaxed bundles shortened evenly (in the I bands) when their lengths were reduced. In early experiments when 5 mM ATP relaxing solution was used to relax the myofibrils, transient nonuniform contractions often damaged the preparations. Therefore, the ATP concentration was set to 15 mM in relaxing and activating solutions.

Active contraction

Myofibril bundles were activated by flowing activating solution, containing 15 mM Mg-ATP and ~30 μM free calcium, through the chamber. The video images provided a useful method to categorize the homogeneity of the individual sarcomeres during contraction. In approximately 50 experiments, ~35 of the myofibril bundles remained attached to the wires and 28 of those maintained clear striation patterns during active contraction. With some preparations, the sarcomeres shortened rather uniformly due to series compliance in the glued ends, but there was no appreciable stretching of any of the visible sarcomeres. At

the plateau of contraction, the sarcomere lengths became steady (Fig. 2 *D*). In other experiments, some of the sarcomeres elongated and the striation pattern became clearly disordered (Fig. 2 *F*). We term these types of responses uniform and nonuniform for the remainder of this paper, although the uniform patterns did show some disorder relative to the relaxed pattern.

Maintenance of a uniform striation pattern in activating solution depended on the sarcomere length before activation. In 13 bundles that began at 2.6 μm or below, 11 bundles (85%) contracted uniformly. In 15 bundles stretched to initial sarcomere lengths above 2.6 μm, only 3 (20%) stayed uniform when activated. Thus, we could not obtain reliable mechanical measurements on bundles at long sarcomere lengths.

Sarcomeres could be readily resolved in the video signals in both relaxing (Fig. 2 *A*) and activating (Fig. 2 *B*) conditions. In Fig. 2, *A* and *B*, brighter regions are plotted upward, so the I bands appear as peaks. The shortening of the sarcomeres during activation can be appreciated by comparing Fig. 2 *A* with 2 *B* (video signals) or Fig. 2 *C* with 2 *D* (phase images). The decrease of sarcomere length when the bundles produced active force was mainly due to compliance at the ends of the preparations because the electronic feedback clamped the wire positions constant. In 13 uniform bundles with clear video signals, sarcomere length decreased 16 ± 2% (mean ± SEM), indicating the presence of considerable series compliance at the attachment points.

Active isometric force

When the solution flow was switched from relaxing (10 mM EGTA) to activating (~30 μM calcium) solution, the force rose after a period of approximately 2 s (Fig. 3). Bundles typically developed ~0.70 μN of force, which was maintained until the inflow was switched back to relaxing solution. The bimodal force development during the first contraction in Fig. 3 was probably caused by nonuniform mixing of the solutions, which occurred occasionally. The downward spike during each contraction in Fig. 3 was caused by imposed length perturbations to be described later.

Force generally declined in successive contractions of a bundle. On average, the force in the fifth trial was 77 ± 4% (mean ± SEM; n = 10) of that in the initial trial. Except for this run-down, the force transients produced by activation/relaxation trials were reproducible in uniform bundles. When the active striation pattern was nonuniform, the force values were highly variable between bundles and sometimes no appreciable force was produced.

Maximal force over the tension baseline was determined from the chart recording of the first contraction from each bundle and divided by the cross-sectional area (see Materials and Methods). Average force per cross-sectional area was 156 ± 18 kN/m^2 (mean ± SEM, n = 8; sarcomere length range, 1.9 to 2.4 μm).

To check that activating solution (30 μM calculated free [Ca^{2+}]) fully saturated the Ca^{2+} regulatory system, a control experiment was performed (Fig. 4) comparing the standard solution with one containing 100 μM excess calcium above the EGTA concentration (free [Ca^{2+}] ≈ 130 μM). The active force gradually declined, but the normal activating solution (circles in Fig. 4) produced the same force as the ~130 μM Ca^{2+} solution (diamonds), indicating that the free [Ca^{2+}] in the normal activating solution was high enough to obtain maximal force. Similar results were obtained in another bundle.

Force-velocity curve

The relationship between the velocity of shortening and force was investigated by applying ramp length changes of various velocities to the activated bundles of myofibrils. At the initiation of each ramp an abrupt length release was also applied to allow the end compliance to shorten. The response of the force to a step-ramp release of moderate velocity could be characterized by four phases shown in Fig. 5 *A*. The force a) dropped rapidly with the step, b) either

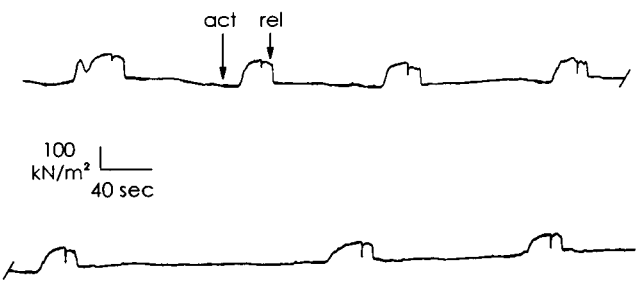

FIGURE 3 Consecutive series of activation and relaxation trials from a bundle of two myofibrils. Times of switching the solution flow to activating and relaxing solutions are indicated by arrows for one of the contractions. The downward spikes during the contractions result from step-ramp releases. Bundle length, 91 μm; cross-sectional area, 6.9 μm^2; relaxed and active sarcomere lengths, 2.2 and 1.9 μm, respectively.

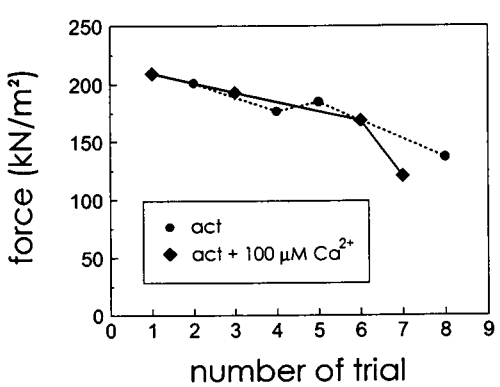

FIGURE 4 Magnitude of contraction in an experiment to test Ca^{2+} saturation of the isometric force. The addition of 100 μM Ca^{2+} to the normal activating solution does not significantly alter the steady isometric force. The decrease in contraction force shown in successive trials is typical. Bundle of two myofibrils; cross-sectional area, 0.77 μm^2.

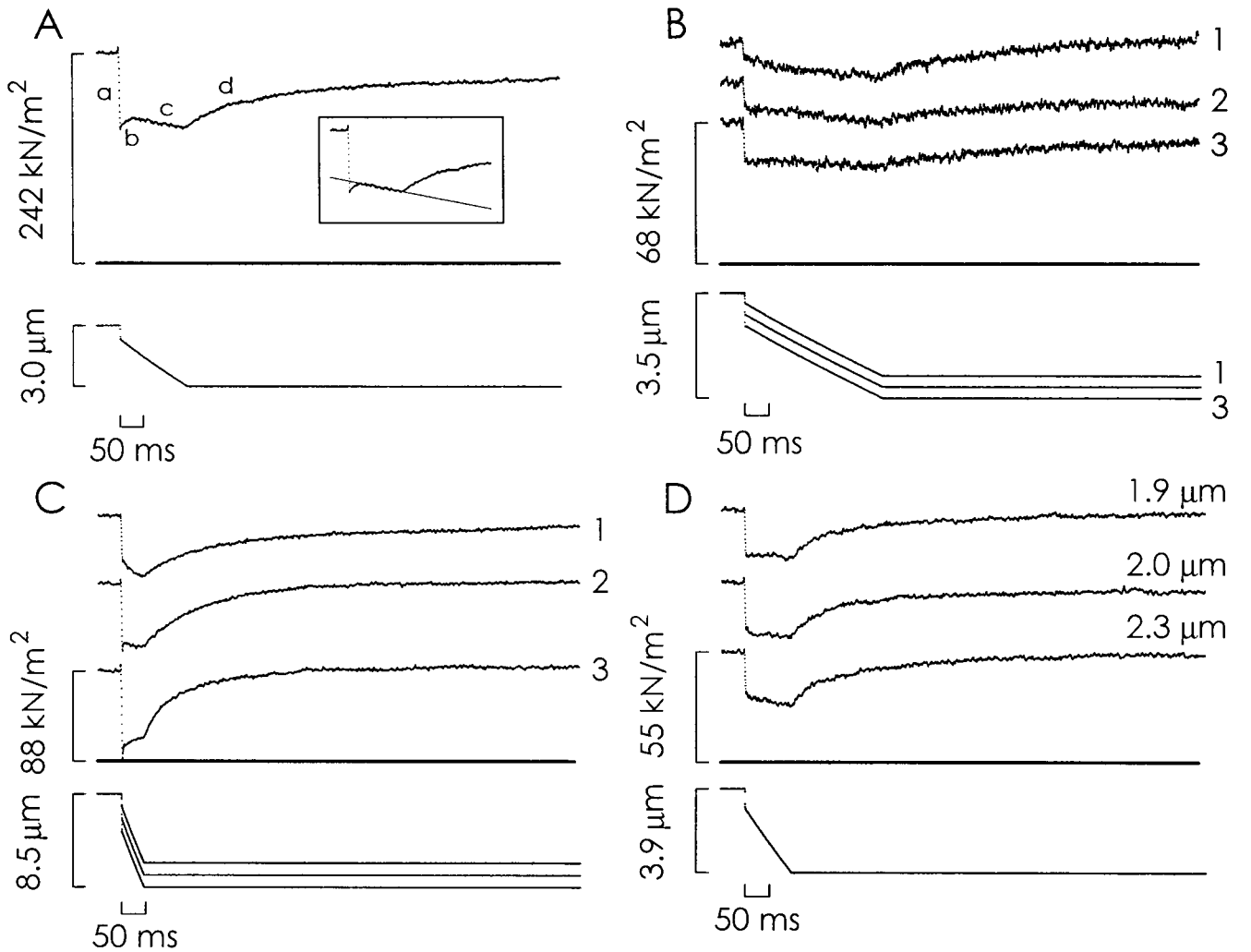

FIGURE 5 Force and length transients from force-velocity experiments. (*A*) The force signal (*upper trace*) is characterized by four phases during and after the step ramp release (*lowest trace*). The middle, flat trace is the zero-force level. The inset shows the method for extrapolating the force during phase c back to the time of the step for plotting force-velocity curves. The bundle is two myofibrils with a length of 101 μm and a cross-sectional area of 5.6 μm^2. (*B* and *C*) Series of three step-ramp releases at two different velocities. The transient, phase b, can be nearly eliminated by choosing a moderate step size (*middle force trace, middle length trace*). The bundle in *C* is two myofibrils with a length of 93 μm and a cross-sectional area of 6.3 μm^2. (*D*) Step-ramp releases applied at three different starting sarcomere lengths. The slope of phase c does not depend on sarcomere length. The bundle is two myofibrils with a cross-sectional area of 6.3 μm^2. The upper two tension traces in *B*, *C*, and *D* have been shifted upward for clarity.

recovered slightly or continued to decrease for ~10 ms, c) decreased linearly for the remainder of the ramp, and d) began to recover immediately after shortening was terminated.

Phase a was interpreted as an elastic response. To determine the source of phase b, series of ramp releases were applied using various amplitudes of the step (Fig. 5 *B* at low velocity; Fig. 5 *C* at high velocity). An optimal step release amplitude reduced or eliminated phase b (tension traces labeled 2 in Fig. 5, *B* and *C*). When the step release was smaller than this optimal value, phase b corresponded to a decrease in force (tension traces labeled 1), whereas a larger step release resulted in partial tension recovery during phase b (Fig. 5 *A* and tension traces labeled 3 in Fig. 5, *B* and *C*). This behavior is consistent with an interaction between the series compliance and the actively shortening sarcomeres. Structures responsible for any series compliance must shorten when the force is reduced from the isometric level to an intermediate level. If the step component of the applied length change does not match the appropriate shortening of those structures, a length readjustment between the series elements and the active component would occupy phase b. Even when the pre-step was set optimally to minimize phase b, the force decreased gradually (phase c) during the ramp. As myofibrillar bundles shortened considerably during the onset of the contraction, many of the contracting bundles were at sarcomere lengths (<2.2 μm) associated with double overlap of the thin filaments in the center of the sarcomere. We considered whether an internal load due to the short lengths might cause the decrease in tension during phase c. To investigate this point, bundles were activated at various starting sarcomere lengths. In the

experiment illustrated in Fig. 5 *D*, the activation trials began at relaxed sarcomere lengths of 2.1, 2.3, and 2.6 μm, and during the maximal force production, the average lengths were 1.9, 2.0, and 2.3 μm, respectively. The decrease of force during phase c was greater at the longest sarcomere length, suggesting that the tension decrease during phase c was not caused by contraction at short length. Similar results were obtained in a second experiment.

A standard procedure was adopted to quantitate force during steady shortening. For velocities greater than ~1.8 μm/s, series of two or more step-ramp releases were applied during successive contractions to optimize the step amplitude. A straight line was fitted to the force during the linear portion of phase c of the optimized trace (inset in Fig. 5 *A*). The force corresponding to the ramp shortening velocity was taken as the intercept of this line at the time of the midpoint of the step. For lower velocities the distinction between phases b and c was more clear. Without optimizing the step amplitude, a straight line was fitted to phase c and back-extrapolated to the mid-point time of the step.

Force responses to step-ramp releases with three to seven different ramp speeds were obtained in nine experiments. Consistent with results from muscle fibers, force during steady shortening decreased as velocity increased (inset in Fig. 6). The value obtained by back-extrapolating phase c of the force response is plotted against ramp velocity in Fig. 6. Each set of the same symbol (e.g., filled squares) corresponds to a different myofibril bundle. The relationship between force and velocity is concave upward and approximately hyperbolic. A least-squares fit of Hill's equation to the data (curve in Fig. 5) yields values V_{max} = 2.3 muscle lengths per second and a/P_0 = 0.37.

We checked whether the run-down of isometric force affected velocity of shortening by comparing the force-velocity relationship measured early in an experiment with the data set obtained near the end of an experiment. After producing eight points for a force-velocity curve, the experiment was extended with a series of 18 additional trials.

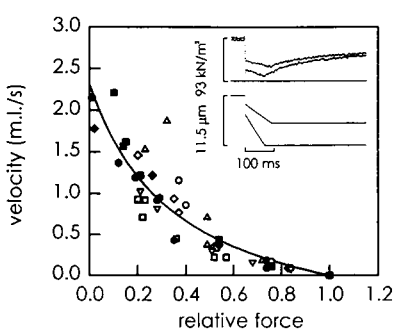

FIGURE 6 Force-velocity curve. Forces are normalized to the isometric value immediately preceding the release. Velocities are given in units of muscle lengths per second (m.l./s.). V_{max}, determined from the intercept of the hyperbolic fit with the ordinate, is 2.3 m.l./s; a/P_o = 0.37. Each symbol corresponds to data from a myofibril bundle. (*Inset*) Force and length transients as in Fig. 5; higher velocity reduces force. Bundle of two myofibrils; length, 70 μm; cross-sectional area, 6.3 μm^2.

Isometric force at the end of the experiment decreased to 18% of the original value, but the force at each velocity, relative to isometric force, hardly decreased. This result indicates that the shortening velocity ran down much less than the isometric force.

Force transients after quick length changes

When rapid length-steps were applied to isometrically contracting bundles of myofibrils (Fig. 7), the force changed suddenly (phase 1) and then recovered toward the isometric value in several components. A partial recovery (phase 2) occurred within the first few milliseconds, and then tension continued to recover on the time scale of tens (phase 3) and hundreds (phase 4) of milliseconds.

The sum of three exponential functions was required to fit the data as described in Materials and Methods. The fitted curves are shown above the data in Fig. 7. The rate constant for the quick recovery, phase 2, was sensitive to the step amplitude in this experiment. The quick recovery was slower for stretch (0.8% of initial length) than for releases and fastest for the largest release (3.4%). The average value of the rate constant for phase 2 recovery was 1510 ± 230 s^{-1} (mean ± SEM; n = 20). There was a high degree of variability in this parameter between experiments and data taken from the whole series did not show a correlation between the size of the step and this rate constant.

Rate constants for phases 3 and 4 averaged 60.1 ± 12.5 s^{-1} (mean ± SEM; n = 22), and 5.37 ± 0.53 s^{-1} (mean ± SEM; n = 19), respectively. The numbers of trials included in these statistics were different because a few values were excluded from the population when the uncertainties of the fitted values, based on the χ^2 values of the fitted curves, were greater than the rate constants themselves. No correlation was found between the rate constants for phase 3 or 4 and the magnitude of the step.

The fitted curves were also used to estimate the force deflection after the length step for determining the stiffness of each preparation. Experiments were included in this group when the length and force transducers had step responses (5–95%) of 500 μs or better. At 500 μs after initiation of the length change, force values were taken from the fitted curves and plotted against the magnitude of length change (Fig. 8). The force-extension curve of the preparations are roughly linear over the range +2.1% to −2.2%. A straight line fitted to this region intercepts the abscissa at a length change of −2.87%. For larger releases, the force-extension curve is more shallow. In some experiments the force values could be taken at earlier times (320–360 μs) from the fitted curves, and the force-extension relations were slightly steeper.

The recovery processes after length changes in Fig. 8 imply active regeneration of force after a length change. However, dynamics of the optoelectronic servos or viscoelasticity in the bundle attachments might also cause apparent recovery of the force signal after a length step. We

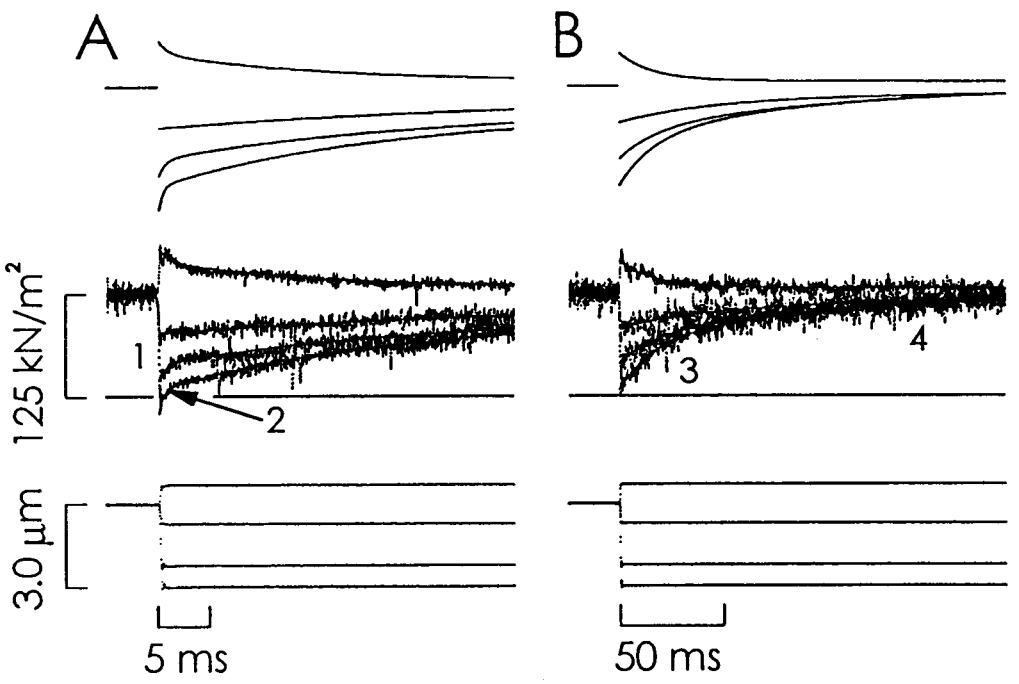

FIGURE 7 Force transients initiated by quick length changes. Tension (*middle, noisier traces*), length transducer positions (*lower traces*), and multi-exponential fitted decays (*upper traces*) are shown at two different time bases in *A* and *B*. Thin, flat traces are the zero-force level. The applied length changes were +0.8, −0.8, −2.6, and −3.4% of the initial length. The sum of two decaying exponential components (phases 3 and 4) is fit to the data in *B*, and a third, faster exponential decay (phase 2) is added in *A*. Bundle of two myofibrils; length, 88 μm; cross-sectional area, 4.6 μm^2; relaxed and active sarcomere lengths, 2.13 and 2.06 μm, respectively.

checked whether force recovery during contraction is related to active energy transduction by comparing responses of the myofibrillar preparations with length changes during active contraction with those in rigor. Fig. 9 *A* shows typical force transients after a release was applied in active contraction (top trace) and the response to the same size step, both stretch and release, given when the myofibrillar bundle was in rigor. The quick recovery observed in active contraction is completely eliminated in rigor, confirming that phase 2 is a property of active contraction. When recordings were made on a much slower time scale (Fig. 9 *B*), a small amount of stress relaxation (slow partial recovery of tension toward the pre-step level) was observed over several seconds. This stress relaxation seems to be located in the glue or at the interface between the glue and the myofibril. Its rate is too slow to appreciably alter the kinetics or extent of the force recovery during active contraction.

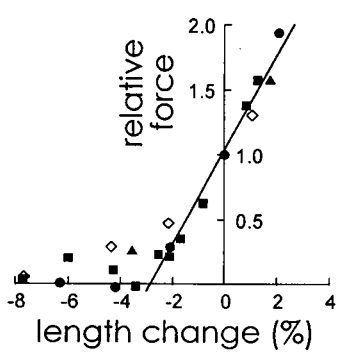

FIGURE 8 Force-extension curve for bundles of two to three myofibrils. Force is normalized to the isometric value immediately preceding the length change. Percent length changes are calculated from the isometric length, which is constant for each experiment. Each symbol corresponds to data from a myofibril bundle. The straight-line fit to the data from +2.1 to −2.2% intercepts the abscissa at −2.9%.

DISCUSSION

Advantages and pitfalls of the technique

The myofibrillar preparation has several potential advantages over fiber preparations including shorter diffusion distance, elimination of potential lateral interactions between myofibrils, and visibility of individual sarcomeres. A myofibril is approximately 100-fold smaller in diameter than a fiber and diffusion times scale with the distance squared, implying 10^4-fold faster equilibration of solutes. Diffusion times between the center and the surface for substrate, products and signaling molecules are on the order of 1 s for a muscle fiber and 100 μs for a myofibril. Pate and Cooke (1989) estimated that the balance between ATPase activity within a rabbit skinned muscle fiber and diffusion of products out of the fiber would lead to a 400 μM radial gradient of phosphate concentration between the core and the surface of a skinned muscle fiber. On the same basis, the gradient of substrate or products within a myofibril would be a negligible 0.085 μM.

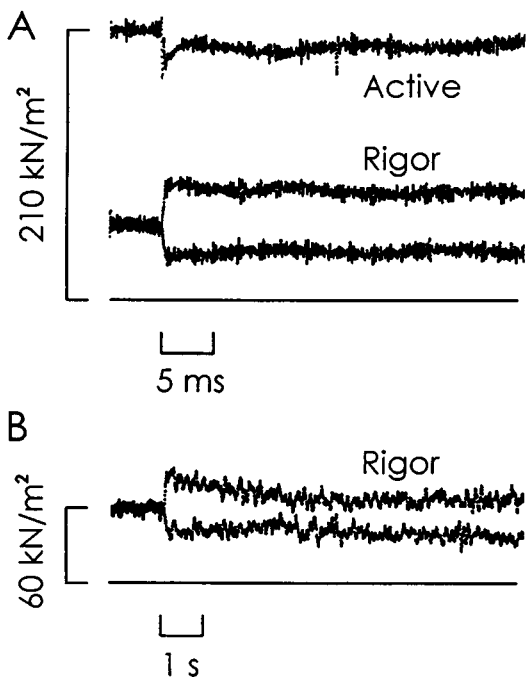

FIGURE 9 Mechanical transients in active contraction (*uppermost trace*) and rigor. The rigor traces are shown on two different time bases in *A* and *B*. Length changes (0.3%) were the same magnitude for each trace. All traces are from the same bundle of three myofibrils; length, 125 μm; cross-sectional area, 4.6 μm^2.

We observed striation spacings of individual sarcomeres in rigor, relaxed, and active conditions, but a higher bandwidth imaging device than our video camera (e.g., a photodiode array) would be required to detect striation spacing changes relevant to quick mechanical transients or to unsteady shortening velocity.

The procedure developed here is more complicated and time consuming than a fiber experiment and the success rate is lower. The attachment method, using silicone glue, added considerable (3–20%) viscoelastic end compliance. For estimating cross-sectional area, we measured the width of the preparation using phase contrast microscopy, which may overestimate the width, possibly by 20% (Linke et al., 1994). With the current set-up, we were not able to measure the thickness of the myofibrillar bundle but judged that most of the bundles were strips of two to three adjacent myofibrils.

The finding that myofibrils, stretched to sarcomere lengths above 2.6 μm in length in relaxing solution, tended to become nonuniform when activated is consistent with sarcomere instability on the descending limb of the sarcomere length-tension curve (Hill, 1953). The nonuniformity prevented us from directly measuring a reliable active length-tension curve.

Active isometric force

The isometric force per cross-sectional area of our myofibrillar preparation was 156 kN/m^2 at 19–23°C. Bartoo et al. (1993) reported a value of 590 kN/m^2 from rabbit psoas myofibrils at 20–22°C; Linke et al. (1994) found 145 kN/m^2 at 20–22°C from myofibrils derived from rabbit myocardium; and Colomo et al. (1995) found a value of 430 kN/m^2 in frog skeletal myofibrils at 15°C. Skinned fibers from rabbit muscle produce forces ranging from 168 to 250 kN/m^2 at temperatures of 15–25°C (Moss, 1982; Crowder and Cooke, 1984; Dantzig and Goldman, 1985; Hibberd et al., 1985; Dantzig et al., 1991; Higuchi and Goldman, 1991; Wang et al., 1993).

The average force obtained in the present work is somewhat lower than those reported in most of the other studies. Protein extraction during storage or the mechanical disruption produced by the homogenization may account for some degradation of performance. The greatest contribution to uncertainty of our force data is the estimation of cross-sectional area. Linke et al. (1994) reported that phase microscopy leads to 20% overestimation of the diameter, and thus the actual force per cross-sectional area may be ~40% higher than we calculated. However, the bundle may contain extra myofibrils situated out of the viewing plane. One extra myofibril above two detected would reduce actual force per cross-sectional area by 33%. Therefore, the force is in the range 105–220 kN/m^2.

Two other minor corrections that could be considered when comparing the present results with earlier myofibril and fiber studies are the ATP concentrations and the nonmyofibrillar area of fibers. [Mg-ATP] in the present study was 15 mM, which decreases fiber force by 5–15% relative to force at the more common 5 mM MgATP (Cooke and Bialek, 1979; Ferenczi et al., 1984). In fast frog and guinea pig muscle fibers, the myofibrils occupy approximately 80–90% of the total cross section (Eisenberg and Kuda, 1976; Mobley and Eisenberg, 1975), so nonmyofibrillar area is not a major correction.

Bartoo et al. (1993) concluded that the high force per cross-sectional area they obtained in skeletal myofibrils implies local calcium concentration variations within intact fibers during contraction and substantial build-up of reaction products within active skinned fibers. The present results do not support these conclusions. Although considerable effort was invested by Bartoo and colleagues in its validation, the cross-sectional area measurement may still be the greatest source of uncertainty in their work, as well as in the present experiments. Another argument against major differences between fibers and myofibrils in isometric contraction is that the ATPase rates are similar (Herrmann et al., 1994).

Considering the various sources of uncertainty, we conclude that the data support the hypothesis that force per cross-sectional area measured in a muscle fiber is derived from a straightforward summation of the myofibrillar force.

Force-velocity relation

Step-ramp releases, used to measure shortening velocity, initiated force transients characterized by several phases,

suggesting interactions between the end compliance and the contractile properties of the myofibrils (Fig. 5 *A*). The continued decrease of force during phase c of shortening indicates non-steady-state behavior, as is often seen in skinned fiber studies and is possibly caused by an increasing internal load (Brenner, 1986). Assuming that the continued force decrease is caused by an internal load that develops as shortening progresses, we extrapolated the force curve back to the time of the beginning of shortening.

The relationship between force and velocity was found to be concave upward, and a fit of Hill's hyperbolic equation to the data yielded values of V_{max} = 2.3 muscle lengths per second (ML/s) at 18–24°C, and the shape factor a/P_o = 0.37. Measurements of V_{max} on untethered myofibrils have ranged between 3 and 10 ML/s (Harada et al., 1990; Harrington et al., 1990; Ohno and Kodama, 1991; Ma and Taylor, 1994). Crowder and Cooke (1984) found V_{max} in skinned psoas muscle fibers under similar conditions to be 5.30 ML/s at 25°C. Wang et al. (1993) obtained 4.5 ML/s at 18–20°C. Many other studies report V_{max} values in fibers ranging from 0.9 to 2.88 ML/s at 10–15°C (Cooke and Bialek, 1979; Moss, 1982; Reiser et al., 1985; Cooke et al., 1988; Wang et al., 1993). Shortening velocity is markedly temperature sensitive (Ranatunga, 1982; Ranatunga and Wylie, 1983). As with our isometric force measurements, the velocity is slightly lower than the typical values found in fibers, possibly due to differences in the preparation of the fibers and myofibrils. Values of a/P_o are not usually reported in the rabbit psoas fiber studies, but our value of 0.37 is somewhat higher than the value of 0.21 reported by Cooke et al. (1988).

Stiffness

Nonlinearity of the immediate force-extension curve (Fig. 8) is a feature of intact muscle fibers (Ford et al., 1977) and is mainly due to truncation of the step response by quick recovery during the short time required to apply the length step. The truncation phenomenon may partly explain the present nonlinearity, but a major factor is probably also nonlinearity of compliance at the attachment points between the myofibril bundle and the wire loops.

An extrapolation of the linear part of the force-extension curve intercepts the zero-force axis at a length step of ~3% of the bundle length, whereas in the most reliable muscle fiber experiments the intercept has been found to be 0.3% in frog intact single fibers (Lombardi et al., 1992) and 0.4% in rabbit skinned fibers (Brenner et al., 1982). In the fiber studies compliance at the ends is functionally eliminated, whereas it is present in our measurements and significantly contributes to the total compliance of the preparation.

Myofibrils contracted approximately 20% when tension developed from the relaxed to the active isometric level. The difference between the 3% extrapolated length change necessary to reduce active force to zero and the 20% shortening measured during the onset of contraction can be explained if the silicone glue at the attachment points exhibits slow viscoelasticity on the slow (seconds) time scale of force development. The observation that length steps in rigor show negligible quick recovery (Fig. 9) indicates that the viscoelastic response of the glue is slow.

Force transients

Force transients after quick length changes in myofibrils (Figs. 7 and 9 *A*) have many similarities with transients measured from muscle fibers. Our observation of significant kinetic components of myofibrillar force recovery, with apparent rate constants extending from 5 s^{-1} to 1500 s^{-1} after quick length changes, conflicts with the finding of Iwazumi (1989) that the plot of stiffness versus frequency from his myofibril preparation was virtually flat above 50 Hz. Iwazumi's myofibrils may have been damaged during preparation because the apparatus was apparently capable of detecting higher frequency components.

Phase 2 of the force transients

In our experiments, the rate constant for quick tension recovery after a length step was 1500 s^{-1} (18–24°C) from an exponential curve fitted to the tension transients. The rate constant reported for phase 2 recovery ranges from 600 s^{-1} (Abbott and Steiger, 1977) to 2600 s^{-1} (Kawai and Zhao, 1993) in rabbit skinned psoas fibers under conditions similar to ours (see also Irving et al., 1995) and 200-1200 s^{-1} for frog intact single fibers at 4°C (Huxley and Simmons, 1971). The rate of recovery in fibers is dependent on the size of the release (Huxley and Simmons, 1971; Abbott and Steiger, 1977), but there was no discernible trend in the present data, possibly because of high scatter. In some myofibrillar bundles a clear strain dependence of the recovery rate was observed (Fig. 7), but the ~3% series compliance probably slowed the rate of phase 2 and suppressed the strain dependence in many experiments. Given the result that the mean value of phase 2 recovery obtained from the myofibrils falls within the rates found in fibers, the mechanism governing phase 2 is probably the same in two preparations.

Phase 3

An exponential component of tension recovery, with rate constant of 60 s^{-1}, was found in the present experiments. Its amplitude, however, had the same sign as phases 2 and 4, whereas in muscle fibers, the component with a similar rate constant has the opposite sign. Phase 3 in fibers is a delay or reversal of force recovery after quick releases or stretches; in myofibrils phase 3 is a continued recovery with an intermediate rate constant. Kawai and Brandt (1980), using sinusoidal analysis, found the effective rate constant of phase 3 to be 138 s^{-1} at 20°C. Davis and Rodgers (1995) found 91 s^{-1} at 21°C.

Phase 3 for a release in fibers has been interpreted as a detachment of cross-bridges or deactivation of the regulatory system (Huxley and Simmons, 1973). Possible interpretations of the opposite amplitude obtained here are that cross-bridges remain attached longer after the length change than in fibers or that the Ca^{2+} regulatory system is altered or loses a component during isolation of the myofibrils. The considerable series compliance in the myofibrillar preparation is also likely to suppress reversal of tension recovery during phase 3.

Phase 4

Final recovery to near the isometric tension took place with a rate constant of approximately 5.4 s^{-1}. Kawai and Brandt (1980) recorded a comparable component in sinusoidal data at 5.5 s^{-1} (20°C).

Summary and significance

The measurements of myofibrillar isometric force, velocity, and mechanical transients provide support for the customary idea that the force and shortening of the myofibrils sum in a straightforward, parallel, and series manner to establish the macroscopic behavior of a skeletal muscle fiber. If lateral connections between myofibrils in a muscle were negligible and the only significant force transmission were axial, then in fibers with localized damage, such as the rents in patients with Duchenne muscular dystrophy, contraction would tear bundles of myofibrils away from each other and open longitudinal clefts along the length of the fiber. This behavior is not observed; instead, the abnormal myofibrillar structure is localized near the region of membrane damage (Engel et al., 1994). This finding implies that significant active forces are transmitted laterally between myofibrils as well as axially from sarcomere to sarcomere. In the present experiments, we occasionally observed individual myofibrils of a bundle not attached to the transducer wires. During activation, the lateral connections between the main myofibril bundle and these partly decoupled myofibrils noticeably restrained their shortening. Thus, in a uniformly contracting, undamaged muscle, the lateral connections between myofibrils help to maintain regional homogeneity and to carry the forces evenly to the exterior of the cell. The present results suggest that lateral mechanical interactions do not markedly influence myofibrillar contraction except by smoothing out minor local inhomogeneities.

The myofibril presents a useful intermediate level of structural organization for studies of biochemistry and mechanics of contraction. Development of this preparation for detailed mechanical studies and description of its properties is important for future work on developing muscles or those altered by gene transfer or disruption.

We thank Drs. Jody A. Dantzig, Hideo Higuchi, Vincenzo Lombardi, Michael K. Reedy, and Henry Shuman and Mr. Perry Sun for useful discussions and Dr. Robert Stehle for helpful comments on the manuscript. We are grateful to Mr. Marcus Bell for software support and for essential discussions, Mr. Ed Horn and Mr. Joseph Pili for excellent mechanical construction and Ms. Kimberly Dopke for help in preparing the manuscript.

This work was supported by National Institutes of Health grant AR42333 and by the Muscular Dystrophy Association.

REFERENCES

Abbott, R. H., and G. J. Steiger. 1977. Temperature and amplitude dependence of tension transients in glycerinated skeletal and insect fibrillar muscle. *J. Physiol.* 266:13–42.

Bartoo, M. L., V. I. Popov, L. A. Fearn, and G. H. Pollack. 1993. Active tension generation in isolated skeletal myofibrils. *J. Muscle Res. Cell Motil.* 14:498–510.

Brenner, B. 1986. The necessity of using two parameters to describe isotonic shortening velocity of muscle tissues: the effect of various interventions upon initial shortening velocity (vi) and curvature (b). *Basic Res. Cardiol* 81:54–69.

Brenner, B., M. Schoenberg, J. M. Chalovich, L. E. Greene, and E. Eisenberg. 1982. Evidence for cross-bridge attachment in relaxed muscle at low ionic strength. *Proc. Natl. Acad. Sci. USA.* 79:7288–7291.

Colomo, F., N. Piroddi, C. Poggessi, and C. Tesi. 1995. Force measurements in myofibrils from frog cardiac and fast skeletal muscle. *Biophys. J.* 68:239a.

Cooke, R. 1986. The mechanism of muscle contraction. *CRC Crit. Rev. Biochem* 21:53–118.

Cooke, R., and W. Bialek. 1979. Contraction of glycerinated muscle fibers as a function of the ATP concentration. *Biophys. J.* 28:241–258.

Cooke, R., M. S. Crowder, and D. D. Thomas. 1982. Orientation of spin labels attached to cross-bridges in contracting muscle fibres. *Nature.* 300:776–778.

Cooke, R., K. Franks, G. B. Luciani, and E. Pate. 1988. The inhibition of rabbit skeletal muscle contraction by hydrogen ions and phosphate. *J. Physiol.* 395:77–97.

Crowder, M. S., and R. Cooke. 1984. The effect of myosin sulphydryl modification on the mechanics of fibre contraction. *J. Muscle Res. Cell Motil.* 5:131–146.

Dantzig, J. A., and Y. E. Goldman. 1985. Suppression of muscle contraction by vanadate: mechanical and ligand binding studies on glycerol-extracted rabbit fibers. *J. Gen. Physiol* 86:305–327.

Dantzig, J. A., M. G. Hibberd, D. R. Trentham, and Y. E. Goldman. 1991. Cross-bridge kinetics in the presence of MgADP investigated by photolysis of caged ATP in rabbit psoas muscle fibres. *J. Physiol.* 432: 639–680.

Davis, J. S., and M. E. Rodgers. 1995. Force generation and temperature-jump and length-jump tension transients in muscle fibers. *Biophys. J.* 68:2032–2040.

Eisenberg, B. R., and A. M. Kuda. 1976. Discrimination between fiber populations in mammalian skeletal muscle by using ultrastructural parameters. *J. Ultrastruct. Res.* 54:76–88.

Engel, A. G., M. Yamamoto, and K. H. Fischbeck. 1994. Muscular dystrophies: dystrophinopathies. *In* Myology, 2nd ed, Vol. 2. A. G. Engel and C. Franzini-Armstrong, editors. McGraw-Hill, New York. 1133–1187.

Ferenczi, M. A., Y. E. Goldman, and R. M. Simmons. 1984. The dependence of force and shortening velocity on substrate concentration in skinned muscle fibres from *Rana temporaria. J. Physiol.* 350:519–543.

Finer, J. T., R. M. Simmons, and J. A. Spudich. 1994. Single myosin molecule mechanics: piconewton forces and nanometre steps. *Nature.* 368:113–119.

Ford, L. E., A. F. Huxley, and R. M. Simmons. 1977. Tension responses to sudden length change in stimulated frog muscle fibres near slack length. *J. Physiol.* 269:441–515.

Friedman, A. L., and Y. E. Goldman. 1993. Force and force transients in bundles of 1–3 myofibrils from rabbit psoas muscle. *Biophys. J.* 64: 345a.

Friedman, A. L., and Y. E. Goldman. 1994. Active ramp shortening of bundles of 1–3 myofibrils from rabbit psoas muscle. *Biophys. J.* 66:5a.

Friedman, A. L., and Y. E. Goldman. 1995. Mechanics studies of bundles of two to three myofibrils from rabbit psoas muscle. *Biophys. J.* 68:361s.

Goldman, Y. E. 1987. Kinetics of the actomyosin ATPase in muscle fibers. *Annu. Rev. Physiol.* 49:637–654.

Goldman, Y. E., M. G. Hibberd, and D. R. Trentham. 1984a. Relaxation of rabbit psoas muscle fibres from rigor by photochemical generation of adenosine-5′-triphosphate. *J. Physiol.* 354:577–604.

Goldman, Y. E., M. G. Hibberd, and D. R. Trentham. 1984b. Initiation of active contraction by photogeneration of adenosine-5′-triphosphate in rabbit psoas muscle fibres. *J. Physiol.* 354:605–624.

Harada, Y., K. Sakurada, T. Aoki, D. D. Thomas, and T. Yanagida. 1990. Mechanochemical coupling in actomyosin energy transduction studied by *in vitro* movement assay. *J. Mol. Biol* 216:49–68.

Harrington, W. F., T. Karr, W. B. Busa, and S. J. Lovell. 1990. Contraction of myofibrils in the presence of antibodies to myosin subfragment 2. *Proc. Natl. Acad. Sci. USA.* 87:7453–7456.

Herrmann, C., C. Lionne, F. Travers, and T. Barman. 1994. Correlation of ActoS1, myofibrillar, and muscle fiber ATPases. *Biochemistry.* 33: 4148–4154.

Hibberd, M. G., J. A. Dantzig, D. R. Trentham, and Y. E. Goldman. 1985. Phosphate release and force generation in skeletal muscle fibers. *Science.* 228:1317–1319.

Higuchi, H., and Y. E. Goldman. 1991. Sliding distance between actin and myosin filaments per ATP molecule hydrolysed in skinned muscle fibres. *Nature.* 352:352–354.

Hill, A. V. 1938. The heat of shortening and the dynamic constants of muscle. *Proc. Roy. Soc. Lond. Ser. B.* 126:136–195.

Hill, A. V. 1953. The mechanics of active muscle. *Proc. Roy. Soc. Lond. Ser. B.* 141:104–117.

Houadjeto, M., T. Barman, and F. Travers. 1991. What is the true ATPase activity of contracting myofibrils? *FEBS Lett.* 281:105–107.

Huxley, A. F. 1974. Muscular contraction. *J. Physiol.* 243:1–43.

Huxley, A. F., and R. M. Simmons. 1971. Proposed mechanism of force generation in striated muscle. *Nature.* 233:533–538.

Huxley, A. F., and R. M. Simmon. 1973. Mechanical transients and the origin of muscular force. *Cold Spring Harbor Symp. Quant. Biol.* 37: 669–680.

Huxley, H. E. 1969. The mechanism of muscular contraction. *Science.* 164:1356–1366.

Irving, M., T. St. Claire Allen, C. Sabido-David, J. S. Craik, B. Brandmeier, J. Kendrick-Jones, J. E. Corrie, D. R. Trentham, and Y. E. Goldman. 1995. Tilting of the light-chain region of myosin during step length changes and active force generation in skeletal muscle. *Nature.* 375:688–691.

Ishijima, A., Y. Harada, H. Kojima, T. Funatsu, H. Higuchi, and T. Yanagida. 1994. Single-molecule analysis of the actomyosin motor using nano-manipulation. *Biochem. Biophys. Res. Commun.* 199: 1057–1063.

Iwazumi, T. 1987. High-speed ultrasensitive instrumentation for myofibril mechanics measurements. *Am. J. Physiol.* 252:C253–C262.

Iwazumi, T. 1989. Mechanics of the sarcomere. *In* Cardiac Mechanics and Function in the Normal and Diseased Heart. H. Hari, H. Suga, E. Barr, and G. Yellen, editors. Springer-Verlag, Tokyo. 13–22.

Kawai, M., and P. W. Brandt. 1980. Sinusoidal analysis: a high resolution method for correlating biochemical reactions with physiological processes in activated skeletal muscles of rabbit, frog and crayfish. *J. Muscle Res. Cell Motil.* 1:279–303.

Kawai, M., and Y. Zhao. 1993. Cross-bridge scheme and force per cross-bridge state in skinned rabbit psoas muscle fibers. *Biophys. J.* 65: 638–651.

Linke, W. A., V. I. Popov, and G. H. Pollack. 1994. Passive and active tension in single cardiac myofibrils. *Biophys. J.* 67:782–792.

Lombardi, V., G. Piazzesi, and M. Linari. 1992. Rapid regeneration of the actin-myosin power stroke in contracting muscle. *Nature.* 355:638–641.

Lymn, R. W., and E. W. Taylor. 1971. Mechanism of adenosine triphosphate hydrolysis by actomyosin. *Biochemistry.* 10:4617–4624.

Ma, Y-Z., and E. W. Taylor. 1994. Kinetic mechanism of myofibril ATPase. *Biophys. J.* 66:1542–1553.

Mobley, B. A., and B. R. Eisenberg. 1975. Sizes of components in frog skeletal muscle measured by methods of stereology. *J. Gen. Physiol.* 66:31–45.

Moss, R. L. 1982. The effect of calcium on the maximum velocity of shortening in skinned skeletal muscle fibres of the rabbit. *J. Muscle Res. Cell Motil.* 3:295–311.

Ohno, T., and T. Kodama. 1991. Kinetics of adenosine triphosphate hydrolysis by shortening myofibrils from rabbit psoas muscle. *J. Physiol.* 441:685–702.

Pate, E., and R. Cooke. 1989. Addition of phosphate to active muscle fibers probes actomyosin states within the powerstroke. *Pflügers Arch.* 414: 73–81.

Press, W. H., S. A. Teukolsky, W. T. Vetterling, and B. P. Flannery. 1992. Nonlinear models. *In* Numerical Recipes in C: The Art of Scientific Computing, 2nd ed. W. H. Press, S. A. Teukolsky, W. T. Vetterling, and B. P. Flannery, editors. Cambridge University Press, New York. 681–688.

Ranatunga, K. W. 1982. Temperature-dependence of shortening velocity and rate of isometric tension development in rat skeletal muscle. *J. Physiol.* 329:465–483.

Ranatunga, K. W., and S. R. Wylie. 1983. Temperature-dependent transitions in isometric contractions of rat muscle. *J. Physiol.* 339:87–95.

Reedy, M. C., M. K. Reedy, and R. T. Tregear. 1988. Two attached non-rigor crossbridge forms in insect flight muscle. *J. Mol. Biol.* 204: 357–383.

Reedy, M. K., K. C. Holmes, and R. T. Tregear. 1965. Induced changes in orientation of the cross-bridges of glycerinated insect flight muscle. *Nature.* 207:1276–1280.

Reiser, P. J., R. L. Moss, G. G. Giulian, and M. L. Greaser. 1985. Shortening velocity and myosin heavy chains of developing rabbit muscle fibers. *J. Biol. Chem.* 260:14403–14405.

Ruppersberg, J. P., and R. Rüdel. 1983. A simple method for controlling the fluid level in a small experimental chamber during slow and rapid fluid exchange. *Pflügers Arch.* 397:158–159.

Savitszky, A., and M. J. E. Golay. 1964. Smoothing and differentiation of data by simplified least squares procedures. *Anal. Chem.* 36:1627–1639.

Stein, L. A., R. P. Schwarz, Jr., P. B. Chock, and E. Eisenberg. 1979. Mechanism of actomyosin adenosine triphosphatase: evidence that adenosine 5′-triphosphate hydrolysis can occur without dissociation of the actomyosin complex. *Biochemistry.* 18:3895–3909.

Uyeda, T. Q. P., S. J. Kron, and J. A. Spudich. 1990. Myosin step size: estimation from slow sliding movement of actin over low densities of heavy meromyosin. *J. Mol. Biol.* 214:699–710.

Wang, D., E. Pate, R. Cooke, and R. Yount. 1993. Synthesis of non-nucleotide ATP analogues and characterization of their chemomechanical interaction with muscle fibres. *J. Muscle Res. Cell Motil.* 14: 484–497.